the plant journal

SEB Society for Experimental Biology

The Plant Journal (2012) **71**, 173–181 doi: 10.1111/j.1365-313X.2012.04923.x

TECHNICAL ADVANCE

In vivo visualization of RNA in plants cells using the λN_{22} system and a GATEWAY-compatible vector series for candidate RNAs

Johannes Schönberger†, Ulrich Z. Hammes†,* and Thomas Dresselhaus

Cell Biology and Plant Biochemistry, University of Regensburg, Universitätsstrasse 31, D-93053 Regensburg, Germany

Received 30 November 2011; revised 19 January 2012; accepted 20 January 2012; published online 13 April 2012.
*For correspondence (email: ulrich.hammes@biologie.uni-regensburg.de)
†These authors contributed equally.

SUMMARY

The past decade has seen a tremendous increase in RNA research, which has demonstrated that RNAs are involved in many more processes than were previously thought. The dynamics of RNA synthesis towards their regulated activity requires the interplay of RNAs with numerous RNA binding proteins (RBPs). The localization of RNA, a mechanism for controlling translation in a spatial and temporal fashion, requires processing and assembly of RNA into transport granules in the nucleus, transport towards cytoplasmic destinations and regulation of its activity. Compared with animal model systems little is known about RNA dynamics and motility in plants. Commonly used methods to study RNA transport and localization are time-consuming, and require expensive equipment and a high level of experimental skill. Here, we introduce the λN_{22} RNA stem-loop binding system for the *in vivo* visualization of RNA in plant cells. The λN_{22} system consists of two components: the λN_{22} RNA binding peptide and the corresponding box-B stem loops. We generated fusions of λN_{22} to different fluorophores and a GATEWAY vector series for the simple fusion of any target RNA 5′ or 3′ to box-B stem loops. We show that the λN_{22} system can be used to detect RNAs in transient expression assays, and that it offers advantages compared with the previously described MS2 system. Furthermore, the λN_{22} system can be used in combination with the MS2 system to visualize different RNAs simultaneously in the same cell. The toolbox of vectors generated for both systems is easy to use and promises significant progress in our understanding of RNA transport and localization in plant cells.

Keywords: fluorescence microscopy, GATEWAY technology, RNA binding protein, RNA transport, technical advance, λN22.

INTRODUCTION

During the past decade innumerable studies have shown that RNA molecules and their functions are more prevalent, diverse and tightly controlled than were previously thought. In the case of endogenous mRNAs, it became evident that the tight regulation of localized mRNAs provides cells with a molecular mechanism to post-transcriptionally control gene expression of master cellular regulators, both spatially and with precise timing (for a review, see Martin and Ephrussi, 2009). Animal oocytes, stem cells and specialized somatic cells, such as nerve cells, are highly polarized, and it was estimated that up to 10% of all mRNAs are polarly localized in these cells as messenger ribonucleoprotein particles (mRNPs) (King *et al.*, 2005). Large-scale fluorescent *in situ* hybridization experiments of more than three thousand distinct mRNAs in early *Drosophila* embryos recently showed that as much as 70% of mRNAs are localized, suggesting that mRNA localization is not an exception but rather the rule (Lecuyer *et al.*, 2007). Furthermore, this localization broadly correlates with protein localization and function, implicating mRNA localization pathways in the coordination of many cellular processes. The localization of mRNAs thus seems to play a major role in organizing cellular networks by targeting ribosomes, as well as other RNPs, and regulating their activity to specific cellular subdomains, thereby controlling translation spatially (St Johnston, 2005). Very recently it was shown that localization of

mRNA also occurs in prokaryotes, indicating that RNA localization may be a very ancient evolutionary feature (Nevo-Dinur *et al.*, 2011).

Polar localization of mRNA can be achieved by three different mechanisms: (i) local stabilization and regulated degradation of mRNA; (ii) local trapping of an RNA that is diffusing through the cytoplasm; and (iii) active and directed transport of mRNA. Although there are examples for all three mechanisms, the latter is the most common mechanism employed. The transported mRNP complexes form larger structures, which are referred to as RNA transport granules. These granules are transported by motor proteins along microtubules and/or the actin cytoskeleton to their final destination. In addition to the association with the cytoskeleton there is also evidence that mRNA transport and ER trafficking may be coupled (Schmid *et al.*, 2006; Aronov *et al.*, 2007). Before mRNPs reach their final subcellular destination, translation is usually delayed by the recruitment of translational repressors (for a review, see Besse and Ephrussi, 2008). It is currently still impossible to predict the structural requirements or 'zip codes' within a transported RNA molecule. In most cases mRNA localization is mediated by stem-loop structures, found in the 3′ untranslated region (3′-UTR) (Macdonald and Struhl, 1988; Macdonald *et al.*, 1993; Macdonald and Kerr, 1997; Bullock and Ish-Horowicz, 2001). It also appears that RNA binding proteins (RBPs) bind to these stem loops with low affinity, and often a large number of low-affinity interactions, none of which are absolutely essential for localization, are involved in mRNA localization (Arn *et al.*, 2003).

Localized mRNAs often appear in mRNP granules, which are heterogeneous in size and composition. Four types of mRNP granules can be distinguished in higher eukaryotes: (i) germ cell (polar) granules (GGs); (ii) stress or stored granules (SGs); (iii) RNA processing bodies (P bodies or PB granules); and (iv) mRNA transport granules (Moser and Fritzler, 2010). Apart from animal model systems with large and easily accessible egg cells or oocytes, as well as polar cells that can be cultivated such as fibroblasts and neurons, surprisingly little is known about the occurrence, composition and function of localized mRNAs/mRNPs in higher organisms. The study of post-transcriptional events associated with localized RNAs/RNPs and specialized ribosomes have received even less attention in plants, mainly because of inefficient plant-derived *in vitro* systems (Bailey-Serres *et al.*, 2009; Lorkovic, 2009). Most progress in plants has been made on the understanding of the transport of plant virus-derived mRNPs (Sambade *et al.*, 2008). The majority of plant mRNPs reported to date are involved in stress response and mRNA degradation processes in P bodies (reviewed by Xu and Chua, 2011), but little is known about RNA localization in plant cells. Localized protein synthesis at the ER, involving cytoskeleton-associated RBPs, has recently been reported for seed storage proteins in *Oryza sativa* (rice) endosperm (Hamada *et al.*, 2003; Wang *et al.*, 2008; Doroshenk *et al.*, 2009; Crofts *et al.*, 2010), and for actin-organizing factor profilin in growing maize root hairs (Baluska *et al.*, 2000). The first mRNA, encoding an interleukin-1 receptor-associated kinase (IRAK)/Pelle-like kinase, was reported to be stored in pollen and only activated for translation in the egg cytoplasm after fertilization (Bayer *et al.*, 2009). It is very likely that mRNAs encoding IRAK/Pelle-like kinases and other proteins in pollen are transported and localized as mRNPs, for example, to the tube tip or cytoplasmic sperm cell microdomains. In summary, molecular mechanisms regulating the localization and subsequent distribution of mRNAs/mRNPs exist in plants, but their identity and composition is largely unknown.

In situ imaging techniques have been applied successfully to visualize and identify such mRNAs/mRNPs, subsets of small non-coding RNAs (sncRNAs) containing RNPs or specialized ribosomal RNPs (rRNPs), such as ribosomes using fixed animal cells. However, these techniques are difficult to achieve with most plant tissues, as they require proper sectioning and are therefore not amenable for high-throughput studies. Moreover, due to tissue fixation *in situ* approaches don't allow to study RNP dynamics, RNA trafficking and localization processes. The methods, which were successfully applied in the animal field, are in principle also available to visualize RNA dynamics in plants (for a review, see Christensen *et al.*, 2010). However, because of the rigid cell wall and turgor pressure, microinjection of fluorescent probes such as molecular beacons or directly labelled RNA is more difficult to achieve in plant cells than in animal cells. In any case these are mechanically invasive methods that require both specialist equipment and experimental skill, and therefore do not allow for the high-throughput screening of localized RNAs/RNPs in plants. Until now, directly labelled RNA was successfully used to visualize the attachment of *Tobacco Mosaic Virus* RNA to the plant actin/ER network (Christensen *et al.*, 2009). The Pumillio-BiFC system employs genetically encoded reporters that target stem-loop structures, visualized by bimolecular fluorescence complementation (BiFC) (Ozawa *et al.*, 2007). The great advantages of this method are that it is not invasive and its sequence remains unmodified because the reporter proteins are engineered to recognize the target RNA molecule (Cheong and Hall, 2006). The Pumillo-BiFC method has recently been used successfully in plants (Tilsner *et al.*, 2009). The drawback of this method is that it requires a great deal of knowledge about the target RNA, the design of Pumillo variants and additionally is time consuming. Similar drawbacks apply to a very recently published method that requires the design of RNA aptamers that mimic the fluorophore in GFP (Paige *et al.*, 2011).

The methods that appear to be most suitable for high-throughput studies of localized RNAs/RNPs are those that take advantage of RNA stem-loop binding RBPs. These

methods are mechanically non-invasive but require the introduction of foreign RNA sequences, often in multiple repeats to increase sensitivity, which may interfere with target RNA function. The two methods, which are the subject of this paper, are the MS2 system and the λN_{22} system. The coat protein of phage MS2 (MS2-CP) binds a 19-nucleotide (19-nt) RNA stem-loop structure with high specificity and affinity (K_d = 6.2 nM) (LeCuyer *et al.*, 1995). When fused to a fluorescent tag this protein can be used to visualize RNAs (Bertrand *et al.*, 1998). The MS2 system has already been used successfully to study RNA transport in plants (Hamada *et al.*, 2003; Zhang and Simon, 2003; Sambade *et al.*, 2008). The same principle was adapted recently to optimize GFP-based RNA stem-loop reporter systems. λN_{22} consists of a 22 amino-acid peptide ligand from the lambda phage fused to a fluorescent tag (Daigle and Ellenberg, 2007). The λN_{22} protein recognizes a 15-nt RNA stem loop, termed box-B, to which the λN_{22} peptide binds with slightly lower affinity (K_d = 22 nM) than the MS2 CP (Daigle and Ellenberg, 2007). Until now, the λN_{22}/ box-B system has been successfully used in animal cells and fungi (Daigle and Ellenberg, 2007; Lange *et al.*, 2008; Konig *et al.*, 2009), but not in plants.

Here we introduce a two-component GATEWAY™ technology based vector series for the use of both systems – MS2-CP and λN_{22} – in plant cells. These RBPs were fused to CFP, GFP, mVenus or mCherry for high versatility, and to perform co-localization studies with each other or any other RBP, allowing simultaneous visualization of various RNPs. The target RNAs under investigation can easily be introduced by GATEWAY recombination, either in the 5′ or in the 3′ position of corresponding stem-loop structures. We further show that λN_{22}/ box-B can successfully be used to visualize RNPs in plants and demonstrate that λN_{22}/ box-B has considerable advantages over the MS2 system, and is therefore well suited for low-background and high-throughput RNP studies in plants.

RESULTS AND DISCUSSION

Generation of the two-component GATEWAY™ vector series

In order to be able to monitor RNA trafficking *in vivo*, and to set the basis for high-throughput RNA localization screening tools and the simultaneous visualization of multiple RNP components, we set out to adopt the λN_{22} system as an additional tool and to compare it with the MS2 system for use in plants. To be able to fully use both RBPs we created fusions of both proteins with CFP, eGFP1, mVenus or mCherry (Figure 1a). These different tags allow the localization of different RNAs using these RBPs in conjunction with other RBPs within the same cell, and will enable downstream applications like fluorescence resonance energy transfer (FRET) analyses. The SV40 nuclear localization sequence (Kalderon *et al.*, 1984) was introduced at the

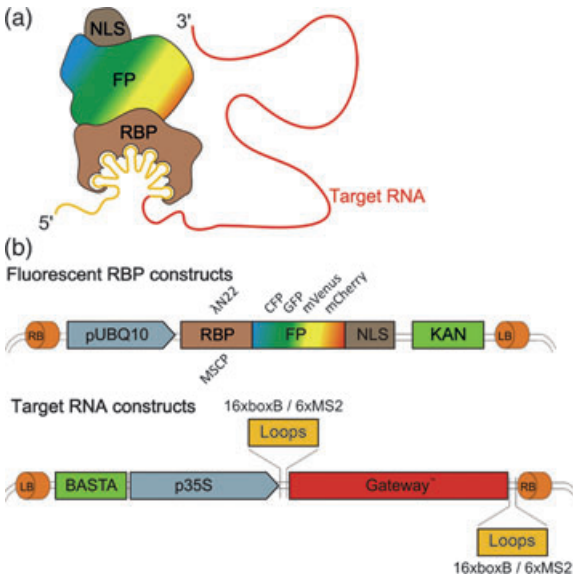

Figure 1. Schematic representation of the two-component RNA visualization systems.
(a) Both systems take advantage of the specific binding of a viral RNA binding protein (RBP, brown) to its corresponding stem-loop structure in the target RNA (here 5′ as an example). The RBPs used are λN_{22} and MS2-CP. These RBPs are fused to a fluorescence protein (FP: CFP, GFP, mVenus or mCherry) containing the SV40 NLS.
(b) Schematic representation of the two-component system vector series. The T-DNA region between left border (LB) and right border (RB) is shown. The RBP-FP-NLS fusion proteins are under the control of the *UBQ10* promoter of Arabidopsis. Stable transformands can be identified by kanamycin selection. Candidate RNAs can be recombined by GATEWAY technology either in the 5′ or 3′ position of the corresponding target RNA stem loops. To enhance the signal strength, six MS2 repeats and 16 box-B repeats were used, respectively. The expression of the resulting RNA molecule is controlled by the cauliflower mosaic virus *35S* promoter. Stable transformands can be selected by BASTA.

C-terminal position in all cases to ensure nuclear localization of the fluorescent RBP when it is not bound to a target RNA, thus enabling background-free visualization of target RNAs in the cytoplasm. These fusion proteins are expressed under control of the *ubiquitin 10* promoter of Arabidopsis (*UBQ10*), which allows strong expression when transiently expressed and which can also be used for constitutive expression after stable transformation (Grefen *et al.*, 2010). In order to enable stable transformation of plants the fluorescent RBP vectors are available with a kanamycin selection marker (Figure 1b).

The RBP target RNA stem loops were cloned in either the 5′ or the 3′ position of the GATEWAY™ cassette (Figure 1b). In order to increase the signal strength we used six repeats of the MS2 stem loops and 16 repeats of the box-B stem loops. Candidate RNAs can easily be introduced by GATEWAY recombination cloning. The transcription of target RNAs is controlled by the cauliflower mosaic virus *35S* promoter (Benfey and Chua, 1989), and the stable transformation of plants using this vector series is possible by BASTA selection. As it was shown that the nuclear history of an RNA

molecule may play an important role in subsequent transport and localization processes (Giorgi and Moore, 2007), it is advisable to use genomic DNA including both UTRs and introns for the generation of candidate RNA constructs, especially if this information is known for an RNA of interest or is available, e.g. from TAIR (Lamesch *et al.*, 2010).

The different selection markers of RBP and target stem loops enable the combination of the two components by transformation or by the crossing and direct selection of the offspring on both selective agents. All constructs were tested and are functional after transient expression in *Nicotiana benthamiana* (tobacco), as described below. Upon email request all vectors described in this manuscript will be made available for academic research purposes, without charge.

Expression of fluorescent RBPs in tobacco leaves

In order to test the functionality of the systems, *Agrobacterium tumefaciens* C58C1 harbouring constructs were used to transiently express λN_{22}-GFP-NLS and MSCP-mVenus-NLS by infiltration into *N. benthamiana* leaves. Fluorescence was visible 2 days after infiltration. In the absence of a target RNA both proteins were exclusively localized to the nuclei (Figure 2a, b, e and f). Stronger fluorescence was always observed in the nucleoli. This localization was background free and is the prerequisite to studying the cytosolic path of candidate RNAs. Upon co-infiltration of target RNAs the fluorescence was still strongest in nuclei, but could be additionally observed in the cytoplasm of the cells (Figure 2c, d, g and h), and was frequently seen in cytoplasmic foci (see below). The same pattern was observed for all fluorescent tags used (not shown). In order to demonstrate the specificity of the RNA-binding proteins, we co-expressed λN_{22}-GFP-NLS with an RNA encoding a scorable cytoplasmic marker (tagRFP) lacking stem loops (Figure S1a–c) or containing the MS2 stem loops (Figure S1d–f). Neither mRNA had any effect on the localization of λN_{22}-GFP-NLS. The same results were obtained when we co-expressed MS2-CP with the tagRFP mRNA lacking stem loops (Figure S1g–i) or the tagRFP mRNA containing box-B stem loops (Figure S1j–l). These data are in agreement with previous studies using GFP coupled to the MS2 system in plants (Hamada *et al.*, 2003; Zhang and Simon, 2003), and are comparable with the results obtained for λN_{22} in mammalian cell culture or yeast (Daigle and Ellenberg, 2007; Lange *et al.*, 2008).

In order to rule out that the different distribution of fluorescence within the cell after co-expression of a target RNA was the result of degradation or any other form of modification of the fluorescent RBPs, total protein was extracted from infiltrated leaf discs and analysed by western blotting (Figure 2i). In the absence of a target RNA, λN_{22} could be identified as a single band corresponding to the predicted molecular weight of 31 kDa. MS2-CP was identi-

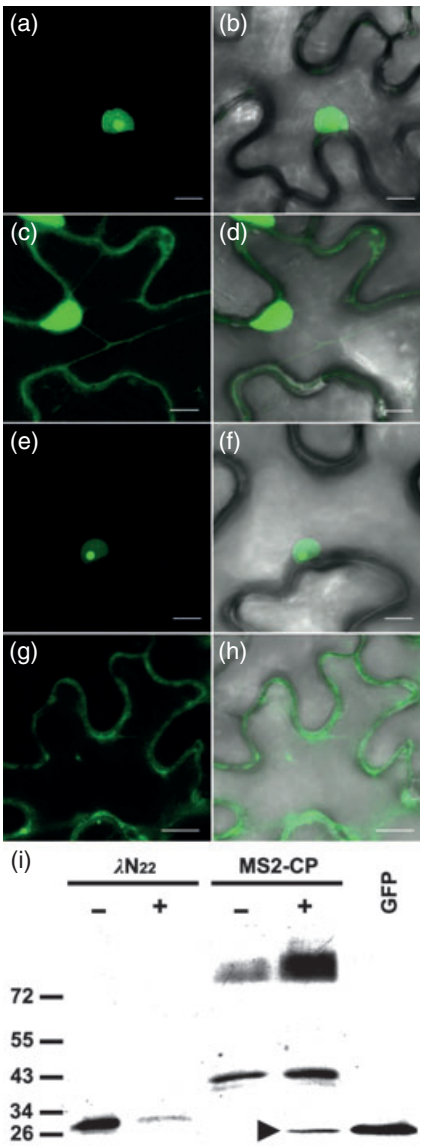

Figure 2. Transient expression of both two-component systems in *Nicotiana benthamiana* leaves.
(a–d) λN_{22}-GFP-NLS.
(e-h) MS2CP-mVenus-NLS. In the absence of a target RNA (a, b, e and f) the fusion proteins localized to the nuclei of epidermis cells. In the presence of a target RNA containing the corresponding target stem loops, fluorescence is readily observed in the cytoplasm (c, d, g and h). a, c, e and g are fluorescent light images. b, d, f and h are overlays of fluorescent light channel and the corresponding bright-field image, so as to highlight the typical jigsaw shape of the *N. benthamiana* epidermis cells. Scale bars: 10 μm.
(i) Western blot analysis of RBP-FP-NLS fusion proteins in the presence (+) or absence (–) of a target RNA. In both cases λN_{22}-GFP-NLS can be detected as a monomer at the predicted molecular weight (31 kDa). In contrast, MS2CP-mVenus-NLS was detected at the predicted molecular weight (43 kDa) in the absence of a target RNA, whereas an additional band corresponding to the size of the free fluorophore was detected in the presence of a target RNA (arrowhead). In the absence or presence of a target RNA an additional band corresponding to the molecular weight of the dimer (~90 kDa) was observed in all samples studied. GFP: free GFP, positive control.

fied as a band corresponding to its calculated molecular weight (43 kDa) and an additional broad band, which was also detected when a target RNA was co-expressed, corresponding to the calculated molecular weight of the MS2-CP dimer. This band was neither observed in protein isolated from λN_{22} leaf discs nor observed in positive control discs (GFP alone), indicating that MS2-CP-mVENUS-NLS may form higher order complexes, preferentially very stable dimers, in the absence and presence of target RNA. This hypothesis is supported by the finding that the broad band was always present even after treating the protein extract with strong reducing agents (data not shown). In the presence of a target RNA we always observed an additional weaker band corresponding to the molecular weight of free GFP (arrowhead in Figure 2i), indicating that MS2-CP-mVenus-NLS is subject to proteolytic degradation in the cytoplasm, which does not occur in the case of λN_{22} in the presence of a target RNA.

Taken together our findings suggest that data obtained with the MS2 system must be interpreted with caution because not all the fluorescence observed in the cytosol is the result of MS2-CP bound to its target RNA. Additionally, higher molecular structures observed with the MS2 system might be artificial, and a result of di-/multimerization of the fluorescent RBP. The fact that these issues do not occur with the λN_{22} system indicates that λN_{22} may be more reliable than the MS2 system, and therefore be used when labelling a single candidate RNA under investigation.

Influence of the position of the stem-loop structure

To further establish the system as a tool to study plant RNPs we wanted to investigate the influence of the position of the stem-loop structures within the target RNA construct on the redistribution of fluorescence and the translation of the target mRNA. To this end we co-infiltrated λN_{22}-eGFP1-NLS or MS2-CP-mVenus-NLS with constructs comprising their corresponding stem-loop structure either in the 5′ or in the 3′ position of the target RNA. In order to easily visualize the translation of target RNAs we used the open reading frame of *tagRFP*, which results in orange-red fluorescence derived from the translated and active protein. As shown in Figure 3, comparable results were obtained with both the λN_{22} and MS2 systems. Regardless of the position of the stem loops we observed fluorescence in the cytosol resulting from RBPs bound to *tagRFP* mRNA. Frequently signals accumulated in cytoplasmic foci (Figure 3a, d, g and j). However, in both systems translation of the target mRNA, indicated by the orange-red fluorescence of tagRFP, was observed only when the stem loops were in the 3′ position of the *tagRFP* gene (Figure 3e and k). As shown in Figure S1 the co-expression of the marker proteins with non-specific tagRFP mRNAs did not lead to a redistribution of fluorescence. Therefore, the presence of marker proteins, as indicated by the fluorescence in the cytoplasm, results from RNA binding and not from non-specific interaction of the marker proteins with tagRFP mRNA. We never detected fluorescence of the translation product when the stem loops were in the 5′ position of the *tagRFP* gene (Figure 3b and h). To rule out the possibility that the failure to observe tagRFP fluorescence was caused by the lack of transcription of the target RNA, we isolated RNA from infiltrated sectors, treated these with DNase and performed oligo dT primed reverse transcriptase PCR. As shown in Figure S2, transcripts were present demonstrating that the absence of tagRFP fluorescence originated from a translation block occurring when the stem loops were in the 5′ position of the tagRFP open reading frame. Translation is probably inhibited because ribosome entry is blocked by the presence of multiple RBP-FP fusion proteins. Alternatively, the 5′ MS2 and box-B stem loops contain several ATG start codons that are not in frame, and may thus serve as translation initiation sites leading to the translation of non-sense peptides.

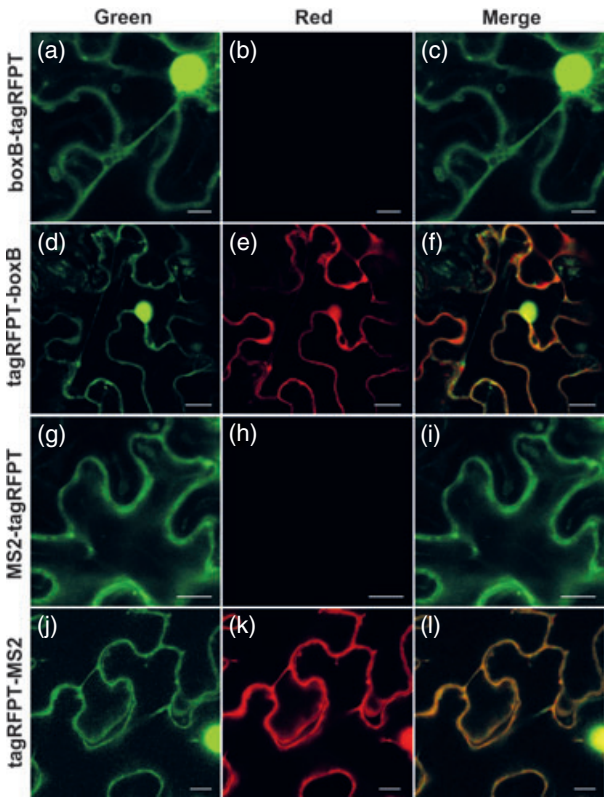

Figure 3. Transient co-expression of λN_{22}-GFP-NLS and MSCP-mVenus-NLS with a target RNA encoding tagRFP as a scorable marker to study the influence of the 5′ and 3′ position of the corresponding stem loops (box-B or MS2) on the translation of the co-expressed RNA.
(a–c) λN_{22}-GFP-NLS and *16 box-B -tagRFP;* (d–f) λN_{22}-GFP-NLS and *tagRFP-16boxB;* (g–i) MS2-CP-mVenus-NLS and *6MS2-tagRFP;* (j–l) MS2-CP-mVenus-NLS and *tagRFP-6MS2*. In all cases the co-expression led to the presence of fluorescence in the cytosol (a, d, g and j). The translation of tagRFP only occurred when the stem loops were in the 3′ position of the tagRFP RNA (e and k), leading to the yellow fluorescence resulting from co-localization in f and l. Scale bars: (d–f) and (j–l), 20 μm; (a–c) and (g–i) or 10 μm.

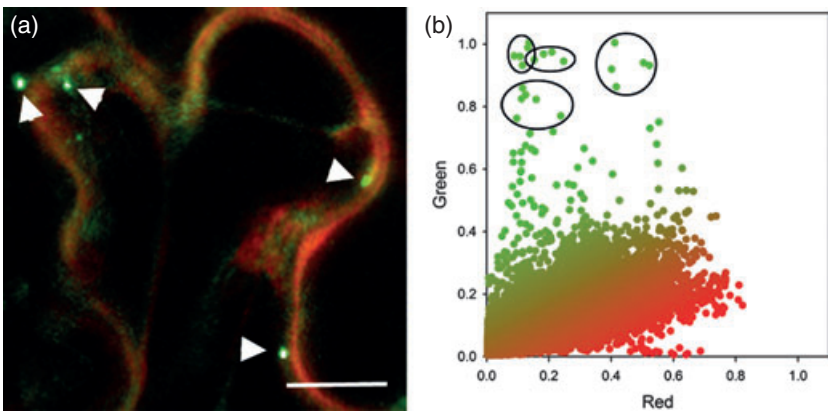

Figure 4. Transient co-expression of λN_{22}-GFP-NLS with a target RNA encoding tagRFP as a scorable marker leads to the presence of green fluorescence in the cytoplasm and the formation of transport granules [arrowheads in (a)].
Fluorescence intensities of each pixel in (a) in the green and the red channel were plotted against each other (b). The four circles highlighted in (b) represent pixels, which are high in green fluorescence and almost free of red fluorescence. These pixels constitute the fluorescent foci/transport granules in (a). These data show that the transport granules are composed exclusively of tagRFP mRNA and RBP. Scale bar: 20 μm

Presence of higher order mRNPs and transport granules

In addition to the presence of fluorescence in the cytosol, upon co-expression of a corresponding target RNA cytoplasmic foci were observed using both systems (Figure 4; Video Clips S1 and S2). These foci were always observed, and formed independently of the type of RNA, i.e. from foreign RNA such as tagRFP or a plant mRNA encoding a cytosolic or secreted protein (data not shown), and thus were independent of translation at free ribosomes or at ribosomes associated with the rough ER. These cytoplasmic foci were rather uniform in size. Their true diameter is difficult to evaluate in fluorescence images; however, based on the images the size of the foci is 800–1200 nm and their motility indicated that they represent mRNP transport granules. These transport granules were highly motile and moved directionally, occasionally in a stop-and-go fashion, indicating an association with a cytoskeletal component rather than simple diffusion (Video Clips 1 and 2). λN_{22} granules moved with a velocity of 0.98 $\pm$ 0.1 μm s^{-1} (n = 5, time series taken in different cells), and MS2-CP particles moved at an average velocity of 0.31 $\pm$ 0.05 μm s^{-1} (n = 5 time series taken in different cells). These data are in good agreement with velocities observed for both systems in yeast, filamentous fungi or the *Drosophila* egg cell, in which the velocities ranged from 400 nm s^{-1} for MS2-CP granules to 1.6 $\pm$ 0.7 μm s^{-1} for λN_{22} granules (Bertrand *et al.*, 1998; Becht *et al.*, 2006; Lange *et al.*, 2008; Zimyanin *et al.*, 2008; Konig *et al.*, 2009). Because we detected extremely stable dimers in our western blot analysis (Figure 2i) we limited the detailed evaluation of the transport granules to the λN_{22} system. When λN_{22}-GFP-NLS and tagRFP- box-B were transiently co-expressed within the same cell, we observed green fluorescence (Figure 3d) resulting from the fluorescent RBP and orange-red fluorescence resulting from the translation of the *tagRFP* mRNA (Figure 3e) within the same cell. Merging both channels resulted in yellowish fluorescence arising from co-localization. Figure 4a shows a section of the cell shown in Figure 3f. It is readily visible that the co-localization was not absolute, i.e. there were domains within the cytoplasm that were exclusively highlighted by red fluorescence, and other domains exclusively highlighted by green fluorescence. The most prominent green foci are labelled with arrowheads, and represent motile transport granules. Fluorescence intensity values of both channels were measured for each pixel in Figure 4a, and were plotted against one another to quantify the green and red fluorescence (Figure 4b). From this illustration it is obvious that there are pixels that are either only red or only green. Among the pixels that display the highest intensities in the green channel is a subset of pixels contained in the circles of Figure 4b. These pixels constitute transport granules marked by arrowheads in Figure 4a. The granules thus did not co-localise with the translation product. In summary, these findings indicate that mRNA is transported within granules. The translation product could be laid down, whereas the particle continues to move or, similar to the situation in yeast or animal cells, translation does not occur in these structures. In order to be translated the granules need to be disassembled, which contributes or gives rise to all of the green fluorescence, which in the case of the epidermal cells appears to be evenly distributed. It will be interesting to see if polar localization within certain cells exists in plants, similar to animal cells, fungi and even bacteria, and how this polarity is brought about. In this case the aforementioned observations, and especially the positioning of the stem loops, has several important implications. If a protein encoded by a target mRNA plays a role in the assembly, transport or polar localization of its own mRNA, a true picture can only be obtained in transient assays once the mRNA can be translated. However, overexpression, especially in transient assays or systems using strong promoters may also result in the accumulation of target RNA-encoded proteins, leading to artefacts. Moreover, if a target RNA under investigation was localized by a 'localized translation mechanism' (for a review, see St Johnston, 2005), the use of a construct with the stem loops

in the 5′ position would fail to detect such a mechanism. On the other hand, if localization signals were contained within the 3′-UTR of the RNA under investigation, the additional stem loops in the 3′ position might mask the correct transport and localization of this RNA. In order to circumvent these obstacles we suggest cloning stem loops in both 5′ and 3′ positions with respect to the RNA under study.

Simultaneous visualization of different RNAs within the same cell

We further investigated whether it is possible to use the λN_{22} and the MS2-CP system simultaneously to visualize two different RNA populations within the same cell. To this end we transiently transformed *N. benthamiana* epidermis cells with four different constructs: λN_{22}-CFP-NLS, MS2-CP-mVENUS-NLS and two different target RNAs containing the corresponding stem loops. As a target for λN_{22} we used an mRNA encoding a plasma membrane localized protein which is translated at the rough ER. As a target for MS2-CP we used an mRNA encoding a cytoplasmic protein, which is translated at free ribosomes. In both cases we used the entire genomic region including UTRs and introns based on the annotations in TAIR 10 (Lamesch *et al.*, 2010). As shown in Figure 5a–c, distinct transport granules could be observed, which indicates that the two systems can be used to simultaneously to monitor two different populations of mRNA. However, it should be mentioned that because of the fairly quick movement of the granules simultaneous tracking of two populations of granules requires patience and sophisticated equipment.

In order to demonstrate that the motile granules observed represent RNA transport granules and to show the use of the λN_{22} system in conjunction with endogenous cytoplasmic RBPs, we co-expressed λN_{22}-mCherry-NLS, a target mRNA and the cytoplasmic RBP At4g17520 fused to GFP. This protein is a member of the hyaluronan/mRNA binding protein family. Members of this family have been shown to be involved in stabilizing mature mRNA in the cytoplasm of animal cells (Heaton *et al.*, 2001). Upon co-expression of the target mRNA encoding a plasma membrane-localized protein (see above) and box-B stem loops in the 3′ position, we observed more green granules derived from cytoplasmic RBP-GFP fusion protein compared with red granules, simply because an RNA-binding protein from plants with low specificity has more targets than the heterologous and highly sequence-specific λN_{22} RBP. We also observed red granules not joined by green granules (arrowheads in Figure 5d–f), which are transported independently. Interestingly, often cytoplasmic foci were found to be composed of green and red granules, which moved together at an average velocity of about 0.5 ± 0.1 μm s^{-1}. This was insignificantly slower than that of the individual red or green granules (0.9 ± 0.1 and 1.4 ± 0.5 μm s^{-1}, respectively; n = 3 individual cells). In all cases the ‘tandem’ granules moved in an oriented, probably cytoskeleton-mediated directional fashion (arrows Figure 5d–f), indicating that the two foci are co-ordinately transported. This suggests that the

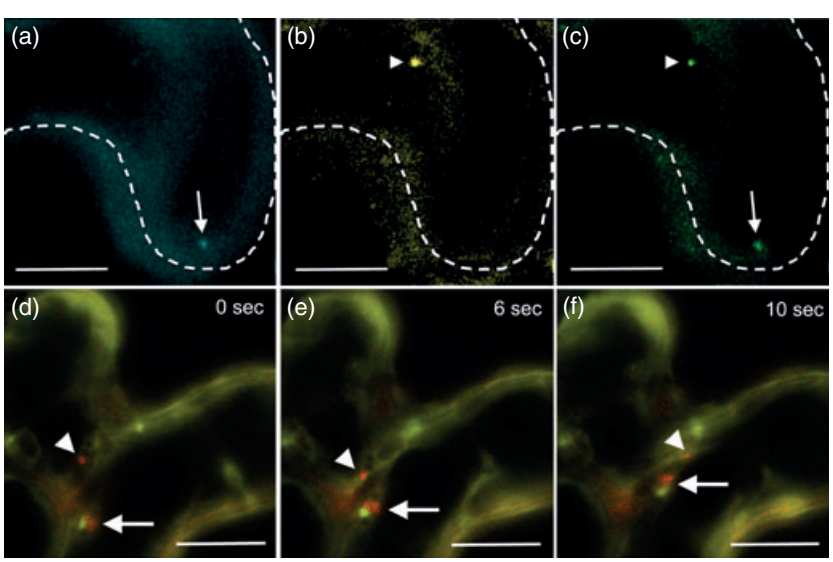

Figure 5. Transient co-expression of λN_{22}-CFP-NLS and MSCP-mVenus-NLS with their target RNAs containing the corresponding stem loops in the same epidermis cell of *Nicotiana benthamiana*.
(a) CFP channel; (b) YFP channel; and (c) overlay of panels (a) and (b). A distinct higher order transport granule containing λN_{22}-CFP-NLS is marked by an arrow in (a) and (c), and a transport granule of MSCP-mVenus-NLS is marked by an arrowhead in (b) and (c). The outline of the cell is represented by a dotted line.
(d–f) Co-expression of λN_{22}-mCherry-NLS, a GFP-labelled cytoplasmic RNA binding protein (RBP) and a target RNA containing box-B stem loops. RNA transport granules consisting of λN_{22}-mCherry-NLS are labelled with an arrowhead. Transport granules consisting of λN_{22}-mCherry-NLS, its mRNA target plus GFP-labelled RBP (arrow) move co-ordinately and directionally together. The times indicated are the real-time observations relative to (d) as the starting point. Scale bars: 10 μm.

coordinated movement is mediated by RNA binding because in the absence of a box-B-containing target, RNA λN_{22} remained in the nucleus, whereas RBP1-GFP granules could be observed at comparable frequencies (arrowheads in Figure S3). The series of pictures shown in Figure 5d–f is also provided as Video Clip S3. The joint movement of viral RBP and the endogenous RBP is very similar to the movement of Staufen RBP and its target *oskar* mRNA tagged with MS2 stem loops and visualized by MS2-CP and co-localized with the Staufen RBP (Zimyanin *et al.*, 2008). In summary, these data show that the λN_{22} system can be used to monitor RNA transport and movement *in vivo*, and additionally could be used to visualize the movement of RNAs in combination with endogenous RBPs.

Conclusion and outlook

In this technical paper we introduced the λN_{22} system as an additional tool to visualize RNA/RNPs and to study their trafficking and dynamics in plant cells *in vivo*. We demonstrated *in vitro* that λN_{22} does not display the possible pitfalls that may be encountered using the MS2-CP system, and may therefore be more reliable. These features may essentially result from the smaller size of the RNA binding component (22 compared with 117 amino acids) of the RBP. Moreover, we provide a vector series and seeds of marker plants for numerous studies involving all kinds of RNAs, such as mRNAs, sncRNAs as well as rRNAs, to investigate, for example, RNP assembly, RNA/RNP transport and movement, translational repression as well as polar RNA localization. Moreover, by combining both systems it is now possible to distinguish between two different RNAs in the same cell including functionally different RNPs such as ribosomes and mRNP granules. It will be interesting to see if these methods can be used to identify polar-localized mRNAs in plants.

EXPERIMENTAL PROCEDURES

Generation of the two component vector series for the λN_{22} and MS2 systems

Open reading frames of λN_{22} and MS2-CP, as well as the corresponding stem loops box-B (16 repeats) and MS2 (6 repeats), were amplified by PCR from the original vectors provided by Michael Feldbrügge (University of Düsseldorf), Jan Ellenberg (EMBL Heidelberg) and Tom Okita (Washington State University). Details of the cloning procedure and primer sequences are available upon request. All constructs were confirmed by DNA sequencing and were functionally tested in transient transformation assays in tobacco (*N. benthamiana*).

Infiltration of tobacco leafs

Infiltration of *N. benthamiana* epidermis cells by *A. tumefaciens* C58C1 was performed essentially as described by Bartetzko *et al.* (2009). Briefly, cultures were centrifuged at 3000 g for 5 min and cells were resuspended in the same volume of infiltration buffer [10 mM $MgCl_2$, 10 mM 2-(*N*-morpholine)-ethanesulphonic acid, pH 5.7, 100 μM acetosyringone], and after incubation for 1 h infiltrated into *N. benthamiana* leaves.

Microscopy

Confocal laser scanning microscopy (CLSM) was performed 48–72 h after infiltration using LSM 510 Meta and LSM 710 microscopes (both Zeiss, http://www.zeiss.com), as well as Leica SP2 and SP5 microscopes equipped with acousto-optic beam splitters. Excitation and emission were at: 405 and 450–500 nm, respectively, for CFP; 488 and 500–530 nm, respectively, for GFP; 514 and 530–560 nm, respectively, for mVenus; 561 and 590–620 nm, respectively, for Tag-RFP; and 543 and 585–615 nm, respectively, for mCherry.

RNA isolation and RT-PCR

Leaf material of infiltrated tobacco plants was sampled into liquid nitrogen and total RNA extracts prepared using the RNeasy Plant Mini Kit (Qiagen, http://www.qiagen.com), according to the manufacturer's instructions. Reverse transcription was performed using the SuperScript® VILO™ cDNA Synthesis Kit (Invitrogen, https://www.lifetechnologies.com).

Protein isolation and immunoblotting

Leaf material from *N. benthamiana* was sampled in liquid nitrogen: 1 g of material was ground in 3 ml of grinding buffer (20 mM HEPES, pH 7.5, 100 mM NaCl, 5 mM $MgCl_2$, 1 mM DTT, 1× Complete Protease Inhibitor; Roche, http://www.roche.com). Crude cell debris was removed by centrifugation at 400 g for 4°C. Protein levels were determined by a Bradford assay and 20 μg of protein from the supernatant was used for western blot analysis using a GFP monoclonal antibody (Roche) in a 1 : 1000 dilution and a 1 : 5000 dilution of horseradish peroxidase-coupled anti-mouse secondary antibody (Santa Cruz Biotechnology, http://www.scbt.com).

ACKNOWLEDGEMENTS

This project was funded by the German Research Council DFG grants DR 334/7-1 and SFB 960. We are grateful to Norbert Sauer and Uwe Sonnewald (University of Erlangen) for granting access to their confocal microscopes. We thank two anonymous reviewers for their constructive and valuable input to improve the article.

SUPPORTING INFORMATION

Additional supporting information may be found in the online version of this article:

Figure S1. Co-expression of the markers with non-target RNAs.

Figure S2. Oligo-dT primed RT-PCR was performed to detect *tagRFP* transcripts (top). Actin (bottom) was used a positive control.

Figure S3. Co-expression of λN_{22}-mCherry-NLS and GFP-RBP1 in the absence of a target RNA containing box-B stem loops.

Video Clip S1. Representative time-lapse film of a cell infiltrated with MS2-CP-mVenus-NLS and a target RNA.

Video Clip S2. Representative time-lapse film of a cell infiltrated with λN_{22}-GFP-NLS and a target RNA.

Video Clip S3. Representative time-lapse film of a cell infiltrated with λN_{22}-mCherry-NLS, RBP-GFP (At4g17520) and a target RNA.

Please note: As a service to our authors and readers, this journal provides supporting information supplied by the authors. Such materials are peer-reviewed and may be re-organized for online delivery, but are not copy-edited or typeset. Technical support issues arising from supporting information (other than missing files) should be addressed to the authors.

REFERENCES

Arn, E.A., Cha, B.J., Theurkauf, W.E. and Macdonald, P.M. (2003) Recognition of a bicoid mRNA localization signal by a protein complex containing Swallow, Nod, and RNA binding proteins. *Dev. Cell*, **4**, 41–51.

Aronov, S., Gelin-Licht, R., Zipor, G., Haim, L., Safran, E. and Gerst, J.E. (2007) mRNAs encoding polarity and exocytosis factors are cotransported with the cortical endoplasmic reticulum to the incipient bud in Saccharomyces cerevisiae. *Mol. Cell. Biol.* **27**, 3441–3455.

Bailey-Serres, J., Sorenson, R. and Juntawong, P. (2009) Getting the message across: cytoplasmic ribonucleoprotein complexes. *Trends Plant Sci.* **14**, 443–453.

Baluska, F., Salaj, J., Mathur, J., Braun, M., Jasper, F., Samaj, J., Chua, N.H., Barlow, P.W. and Volkmann, D. (2000) Root hair formation: F-actin-dependent tip growth is initiated by local assembly of profilin-supported F-actin meshworks accumulated within expansin-enriched bulges. *Dev. Biol.* **227**, 618–632.

Bartetzko, V., Sonnewald, S., Vogel, F., Hartner, K., Stadler, R., Hammes, U.Z. and Bornke, F. (2009) The *Xanthomonas campestris* pv. *vesicatoria* type III effector protein XopJ inhibits protein secretion: evidence for interference with cell wall-associated defense responses. *Mol. Plant-Microbe Interact.* **22**, 655–664.

Bayer, M., Nawy, T., Giglione, C., Galli, M., Meinnel, T. and Lukowitz, W. (2009) Paternal control of embryonic patterning in *Arabidopsis thaliana*. *Science*, **323**, 1485–1488.

Becht, P., Konig, J. and Feldbrugge, M. (2006) The RNA-binding protein Rrm4 is essential for polarity in Ustilago maydis and shuttles along microtubules. *J. Cell Sci.* **119**, 4964–4973.

Benfey, P.N. and Chua, N.H. (1989) Regulated genes in transgenic plants. *Science*, **244**, 174–181.

Bertrand, E., Chartrand, P., Schaefer, M., Shenoy, S.M., Singer, R.H. and Long, R.M. (1998) Localization of ASH1 mRNA particles in living yeast. *Mol. Cell*, **2**, 437–445.

Besse, F. and Ephrussi, A. (2008) Translational control of localized mRNAs: restricting protein synthesis in space and time. *Nat. Rev. Mol. Cell Biol.* **9** 971–980.

Bullock, S.L. and Ish-Horowicz, D. (2001) Conserved signals and machinery for RNA transport in Drosophila oogenesis and embryogenesis. *Nature*, **414**, 611–616.

Cheong, C.G. and Hall, T.M. (2006) Engineering RNA sequence specificity of Pumilio repeats. *Proc. Natl. Acad. Sci. USA*, **103**, 13635–13639.

Christensen, N., Tilsner, J., Bell, K., Hammann, P., Parton, R., Lacomme, C. and Oparka, K. (2009) The 5′ cap of tobacco mosaic virus (TMV) is required for virion attachment to the actin/endoplasmic reticulum network during early infection. *Traffic*, **10**, 536–551.

Christensen, N.M., Oparka, K.J. and Tilsner, J. (2010) Advances in imaging RNA in plants. *Trends Plant Sci.* **15**, 196–203.

Crofts, A.J., Crofts, N., Whitelegge, J.P. and Okita, T.W. (2010) Isolation and identification of cytoskeleton-associated prolamine mRNA binding proteins from developing rice seeds. *Planta*, **231**, 1261–1276.

Daigle, N. and Ellenberg, J. (2007) λN-GFP: an RNA reporter system for live-cell imaging. *Nat. Methods*, **4**, 633–636.

Doroshenk, K.A., Crofts, A.J., Morris, R.T., Wyrick, J.J. and Okita, T.W. (2009) Proteomic analysis of cytoskeleton-associated RNA binding proteins in developing rice seed. *J. Proteome Res.* **8**, 4641–4653.

Giorgi, C. and Moore, M.J. (2007) The nuclear nurture and cytoplasmic nature of localized mRNPs. *Semin. Cell Dev. Biol.* **18**, 186–193.

Grefen, C., Donald, N., Hashimoto, K., Kudla, J., Schumacher, K. and Blatt, M.R. (2010) A ubiquitin-10 promoter-based vector set for fluorescent protein tagging facilitates temporal stability and native protein distribution in transient and stable expression studies. *Plant J.* **64**, 355–365.

Hamada, S., Ishiyama, K., Choi, S.B., Wang, C., Singh, S., Kawai, N., Franceschi, V.R. and Okita, T.W. (2003) The transport of prolamine RNAs to prolamine protein bodies in living rice endosperm cells. *Plant Cell*, **15**, 2253–2264.

Heaton, J.H., Dlakic, W.M., Dlakic, M. and Gelehrter, T.D. (2001) Identification and cDNA cloning of a novel RNA-binding protein that interacts with the cyclic nucleotide-responsive sequence in the Type-1 plasminogen activator inhibitor mRNA. *J. Biol. Chem.* **276**, 3341–3347.

Kalderon, D., Roberts, B.L., Richardson, W.D. and Smith, A.E. (1984) A short amino acid sequence able to specify nuclear location. *Cell*, **39**, 499–509.

King, M.L., Messitt, T.J. and Mowry, K.L. (2005) Putting RNAs in the right place at the right time: RNA localization in the frog oocyte. *Biol. Cell*, **97**, 19–33.

Konig, J., Baumann, S., Koepke, J., Pohlmann, T., Zarnack, K. and Feldbrugge, M. (2009) The fungal RNA-binding protein Rrm4 mediates long-distance transport of ubi1 and rho3 mRNAs. *EMBO J.* **28**, 1855–1866.

Lamesch, P., Dreher, K., Swarbreck, D., Sasidharan, R., Reiser, L. and Huala, E. (2010) Using the Arabidopsis information resource (TAIR) to find information about Arabidopsis genes. *Curr. Protoc. Bioinformatics*, **Chapter 1**, Unit1 11.

Lange, S., Katayama, Y., Schmid, M., Burkacky, O., Brauchle, C., Lamb, D.C. and Jansen, R.P. (2008) Simultaneous transport of different localized mRNA species revealed by live-cell imaging. *Traffic*, **9**, 1256–1267.

LeCuyer, K.A., Behlen, L.S. and Uhlenbeck, O.C. (1995) Mutants of the bacteriophage MS2 coat protein that alter its cooperative binding to RNA. *Biochemistry*, **34**, 10600–10606.

Lecuyer, E., Yoshida, H., Parthasarathy, N., Alm, C., Babak, T., Cerovina, T., Hughes, T.R., Tomancak, P. and Krause, H.M. (2007) Global analysis of mRNA localization reveals a prominent role in organizing cellular architecture and function. *Cell*, **131**, 174–187.

Lorkovic, Z.J. (2009) Role of plant RNA-binding proteins in development, stress response and genome organization. *Trends Plant Sci.* **14**, 229–236.

Macdonald, P.M. and Kerr, K. (1997) Redundant RNA recognition events in bicoid mRNA localization. *RNA*, **3**, 1413–1420.

Macdonald, P.M. and Struhl, G. (1988) cis-acting sequences responsible for anterior localization of bicoid mRNA in Drosophila embryos. *Nature*, **336**, 595–598.

Macdonald, P.M., Kerr, K., Smith, J.L. and Leask, A. (1993) RNA regulatory element BLE1 directs the early steps of bicoid mRNA localization. *Development*, **118**, 1233–1243.

Martin, K.C. and Ephrussi, A. (2009) mRNA localization: gene expression in the spatial dimension. *Cell*, **136**, 719–730.

Moser, J.J. and Fritzler, M.J. (2010) Cytoplasmic ribonucleoprotein (RNP) bodies and their relationship to GW/P bodies. *Int. J. Biochem. Cell Biol.* **42**, 828–843.

Nevo-Dinur, K., Nussbaum-Shochat, A., Ben-Yehuda, S. and Amster-Choder, O. (2011) Translation-Independent Localization of mRNA in E. coli. *Science*, **331**, 1081–1084.

Ozawa, T., Natori, Y., Sato, M. and Umezawa, Y. (2007) Imaging dynamics of endogenous mitochondrial RNA in single living cells. *Nat. Methods*, **4**, 413–419.

Paige, J.S., Wu, K.Y. and Jaffrey, S.R. (2011) RNA Mimics of Green Fluorescent Protein. *Science*, **333**, 642–646.

Sambade, A., Brandner, K., Hofmann, C., Seemanpillai, M., Mutterer, J. and Heinlein, M. (2008) Transport of TMV movement protein particles associated with the targeting of RNA to plasmodesmata. *Traffic*, **9**, 2073–2088.

Schmid, M., Jaedicke, A., Du, T.G. and Jansen, R.P. (2006) Coordination of endoplasmic reticulum and mRNA localization to the yeast bud. *Curr. Biol.* **16**, 1538–1543.

St Johnston, D. (2005) Moving messages: the intracellular localization of mRNAs. *Nat. Rev. Mol. Cell Biol.* **6**, 363–375.

Tilsner, J., Linnik, O., Christensen, N.M., Bell, K., Roberts, I.M., Lacomme, C. and Oparka, K.J. (2009) Live-cell imaging of viral RNA genomes using a Pumilio-based reporter. *Plant J.* **57**, 758–770.

Wang, C., Washida, H., Crofts, A.J., Hamada, S., Katsube-Tanaka, T., Kim, D., Choi, S.B., Modi, M., Singh, S. and Okita, T.W. (2008) The cytoplasmic-localized, cytoskeletal-associated RNA binding protein OsTudor-SN: evidence for an essential role in storage protein RNA transport and localization. *Plant J.* **55**, 443–454.

Xu, J. and Chua, N.H. (2011) Processing bodies and plant development. *Curr. Opin. Plant Biol.* **14**, 88–93.

Zhang, F. and Simon, A.E. (2003) A novel procedure for the localization of viral RNAs in protoplasts and whole plants. *Plant J.* **35**, 665–673.

Zimyanin, V.L., Belaya, K., Pecreaux, J., Gilchrist, M.J., Clark, A., Davis, I. and St Johnston, D. (2008) *In vivo* imaging of oskar mRNA transport reveals the mechanism of posterior localization. *Cell*, **134**, 843–853.

